Supplementary Information

Contents of this document:

• Formulas used for the computation of weighted statistics

• Detailed methods for the dating of snow pit and short core

• Supplementary Figures and Tables

• Additional references cited in the Supplementary Information

Computation of weighted statistics

For the dataset (*x*, *y*) of length *n* and weight coefficients *w*, we use:

Weighted mean: $m_w(x,w) = \frac{\sum_{i=1}^{n} w_i x_i}{\sum_{i=1}^{n} w_i}$

Weighted covariance: $cov_w(x,y,w) = \frac{\sum_{i=1}^{n} w_i (x_i - m_w(x,w))(y_i - m_w(y,w))}{\sum_{i=1}^{n} w_i}$

Weighted correlation: $r_w(x,y,w) = \frac{cov_w(x,y,w)}{\sqrt{cov_w(x,x,w)cov_w(y,y,w)}}$

Regression estimate: $\hat{y}_i = ax_i + b$ where a and b were obtained using Weighted Orthogonal Distance Regression (Boggs et al., 1992).

Weighted standard error of the slope: $\sigma_w(a) = \sqrt{\frac{\frac{1}{n-2}\sum_{i=1}^{n} w_i(\hat{y}_i - y_i)^2}{\sum_{i=1}^{n} w_i (x_i - m_w(x,w))^2}}$

Student's t-distribution threshold: $t_{\alpha,n}$ with α the confidence threshold, and n degrees of freedom

Confidence intervals: $a - t_{\frac{\alpha}{2},n-2}\sigma_w < a < a + t_{\frac{\alpha}{2},n-2}\sigma_w$

Details on snow records dating

In this section, we detail the construction of our age model. The first step was to identify yearly horizons, shown in Supplementary Figure 1. Snow pits and the short core were dated annually using seasonally varying signal of non-sea-salt sulfate or sulfur (peaking in spring) and sodium (peaking in late winter; Sigl et al., 2016). Yearly horizons were counted up from the sulfur fallout of Pinatubo eruption, which peaked in 1993 in Antarctica (Cole-Dai and Mosley-Thompson, 1999).

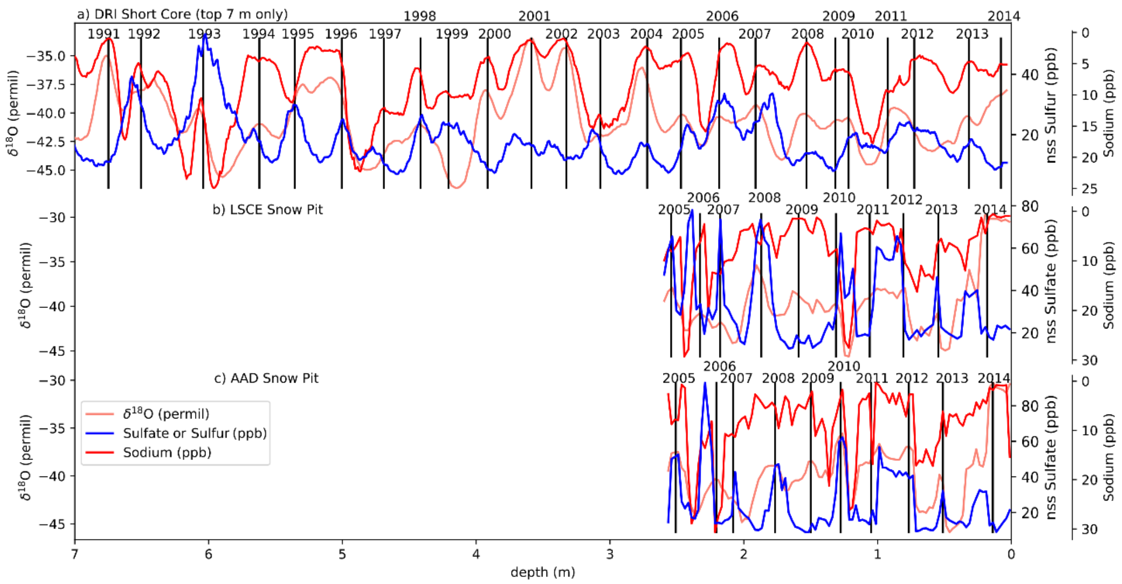

Supplementary Figure 1. Series of $\delta^{18}O$, non-sea-salt sulfur or sulfate and sodium for (a) the top 7 m of the DRI Short Core (including Pinatubo eruption deposit), (b) the LSCE snow pit and (c) the AAD snow pit. Year horizons are shown with vertical black bars. For the LSCE snow pit profile, the sulfate concentration has been measured by ion chromatography at the Institut des Geosciences de l'Environnement (Ginot et al., 2014). Sulfur is shown for the DRI short core instead of sulfates because of the measurement was done with ICP-MS (McConnell et al., 2002).

We then use the $\delta^{18}O$ series to refine the chronology at the seasonal scale, i.e. we do not modify the chronology at the yearly scale but better adjust the seasonal thickness within the different years. The identified year horizons cannot be moved by more than a year in the following process.

With the assumption that the snow pit $\delta^{18}O$ can be modelled using the $\delta^{18}O$ of precipitation, daily precipitation rates and water vapor diffusion within the snow, we refined our dating by a method of peak and mid-slope matching between the measured $\delta^{18}O$ and modelled temperature from MAR or modelled $\delta^{18}O$ from ECHAM5-wiso. In this exercise, temperatures from MAR were converted into $\delta^{18}O$ using a linear transformation of $\delta^{18}\mathrm{O} = a \times \mathrm{T} - \mathrm{b}$, even if we are aware that site differences are expected. Actually, the exact $\delta^{18}O$ values do not matter, as only the relative amplitude of the peaks will influence the diffusion and matching process. We detail hereafter the matching of LSCE snow pit $\delta^{18}O$ to ECHAM5-wiso $\delta^{18}O$.

Because isotopic diffusion smoothens and broadens annual peaks, we simulated a diffusion in the modelled series by converting them to depth using the snowfall rates and then applying a simple vertical diffusion model

$$\frac{\partial \delta^{18}O}{\partial t} = \frac{\partial}{\partial \mathrm{z}}\left(D_f(z) \cdot \frac{\partial \delta^{18}O}{\partial \mathrm{z}}\right)$$

that we simplified to

$$\frac{\partial \delta^{18}O}{\partial t} = D_f(z) \cdot \frac{\partial^2(\delta^{18}O)}{\partial \mathrm{z}^2}$$

with D_f given by Johnsen et al. (2000):

$$D_f(z) = \frac{m \cdot p \cdot D_a}{R \cdot T \cdot \alpha \cdot \tau(z)}\left(\frac{1}{\rho(z)} - \frac{1}{\rho_{ice}}\right)$$

where m is water molar weight in kg·mol^{-1}, p is the saturation vapor pressure over ice in Pa, D_a is the normal diffusivity in air of water vapor in m^2·s^{-1}, R the ideal gas constant, T the temperature in K, α the fractionation factor in water vapor for ^{18}O, τ the tortuosity, ρ the density of the snow and ρ_{ice} the density of the ice.

The depths were converted back into dates using the model dates. Results of the diffusion are shown for δ^{18}O from ECHAM5-wiso in Supplementary Figure 2.

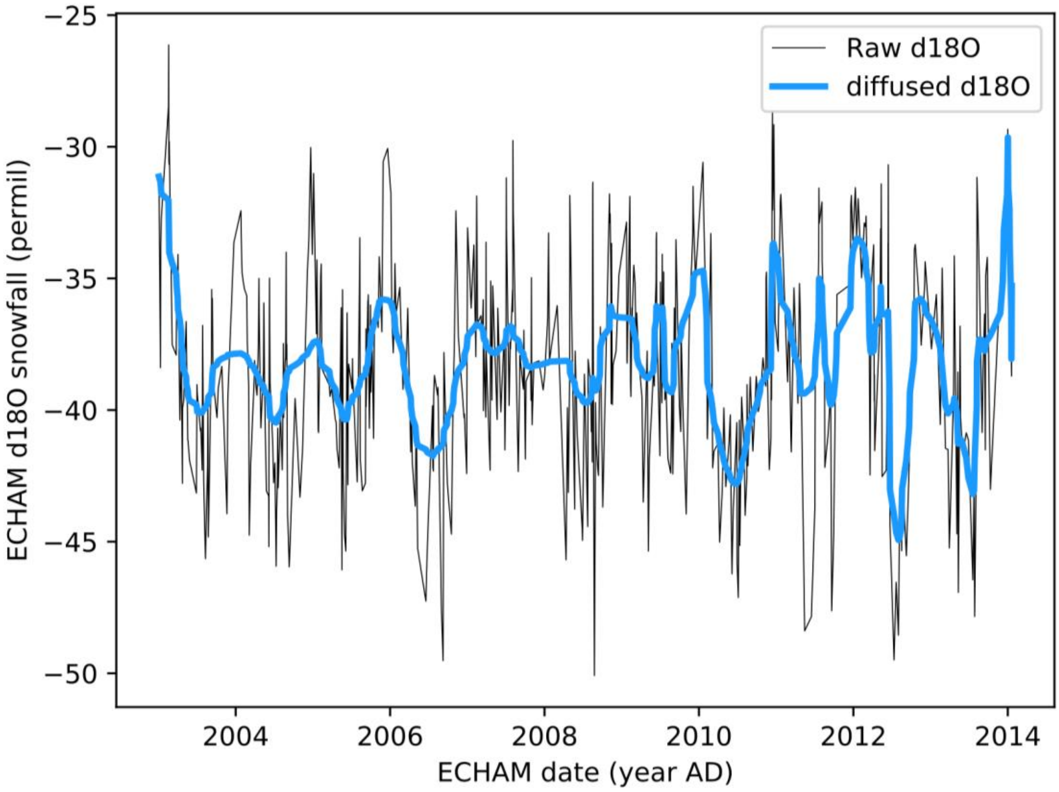

Supplementary Figure 2. Original δ^{18}O in the precipitation from ECHAM5-wiso (thin black line) and diffused δ^{18}O (thick blue line). Note that the recent layers are less affected by diffusion than older layers.

Next, we seek to match the extrema and mid-slope points of the measured δ^{18}O to the diffused δ^{18}O from models, as shown in Supplementary Figure 3.

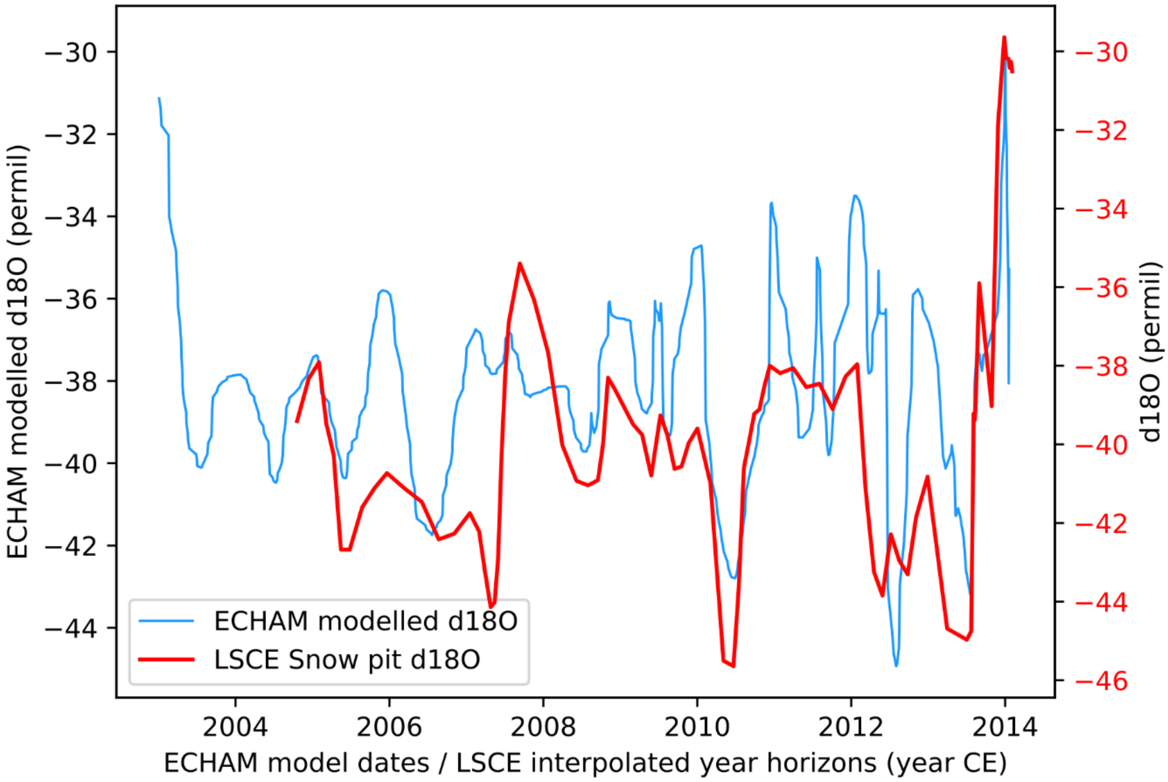

Supplementary Figure 3. Diffused precipitation $\delta^{18}O$ from ECHAM5-wiso, with model dates (blue) and measured $\delta^{18}O$ from the LSCE snow pit, with year-horizon interpolation as the age-model (red).

To better match within a year, we apply a 1-year high-pass filter, by removing the 1-year running mean signal to each $\delta^{18}O$ series. We then detect maximum, minimum, and 0-value crossings for each year, and tie the LSCE $\delta^{18}O$ to the ECHAM $\delta^{18}O$. The tie points on the high-passed filtered series are shown in Supplementary Figure 4. LSCE age values are interpolated between the tie points.

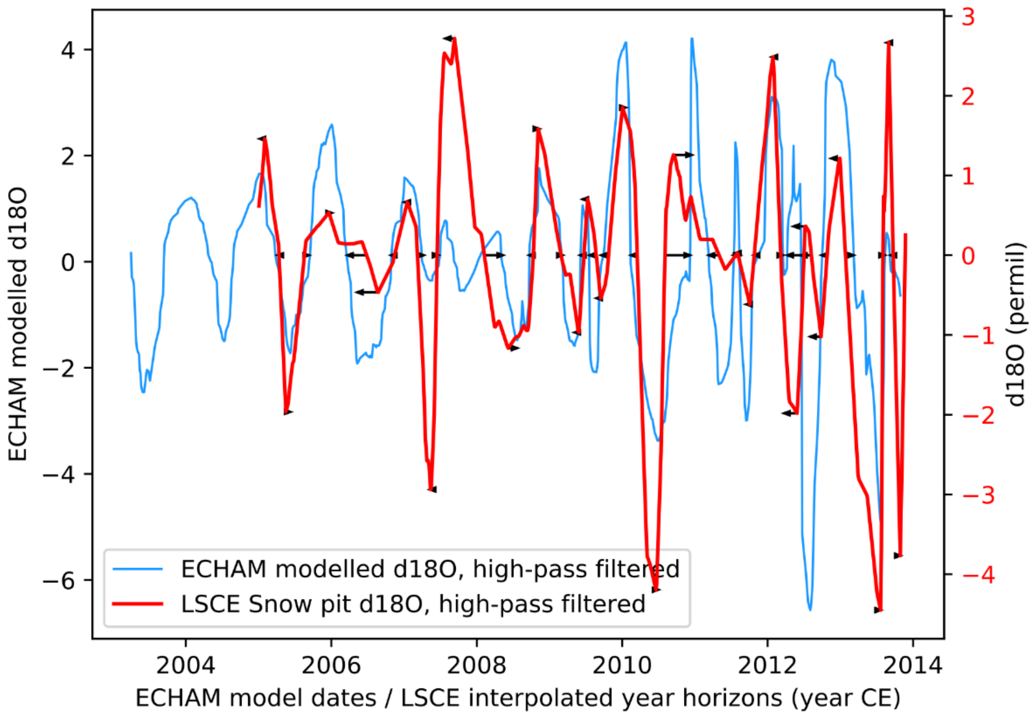

Supplementary Figure 4. One-year high-passed diffused precipitation $\delta^{18}O$ from ECHAM5-wiso, with model dates (blue) and one-year high-passed measured $\delta^{18}O$ from the LSCE snow pit, with year-horizon interpolation as the age-model (red). Peak and 0-value crossings matching is represented by black arrows, pointing where the LSCE snow pit dates were shifted to match the ECHAM5-wiso $\delta^{18}O$.

LSCE Snow Pit $\delta^{18}O$ original values are shown on their old age scale and new age scale in Supplementary Figure 5.

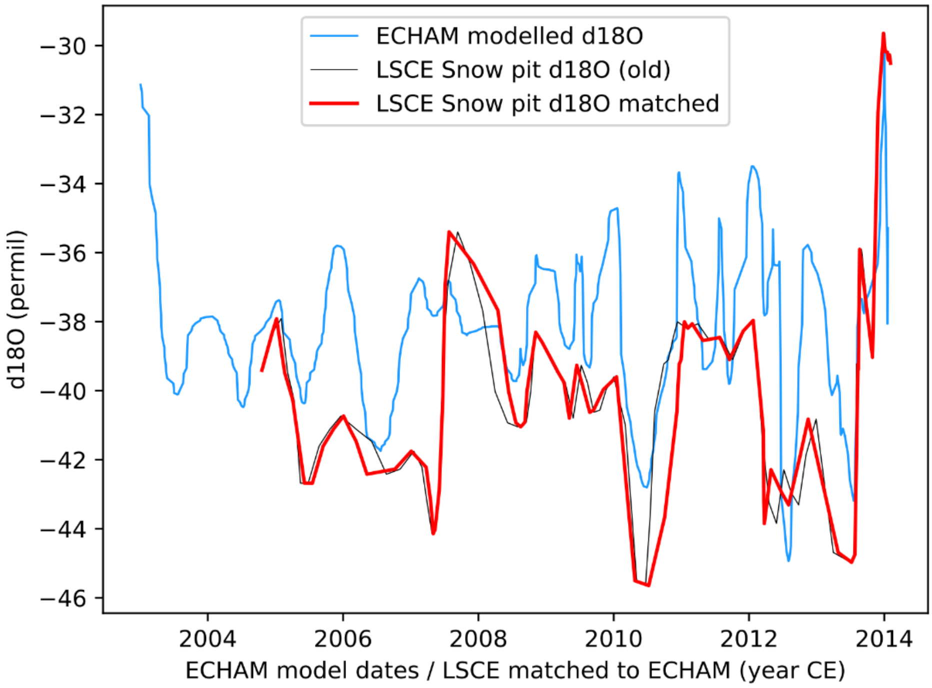

Supplementary Figure 5. Diffused precipitation $\delta^{18}O$ from ECHAM5-wiso, with model dates (blue) and measured $\delta^{18}O$ from the LSCE snow pit, on the year-horizon interpolation age-model (thin black line), and on the newly created age model from the matching (red).

We repeat the same process with MAR temperatures converted to $\delta^{18}O$, resulting in a slightly different age model. The two matched age models are shown in Supplementary Figure 6, alongside the former age model resulting from year-horizon interpolation.

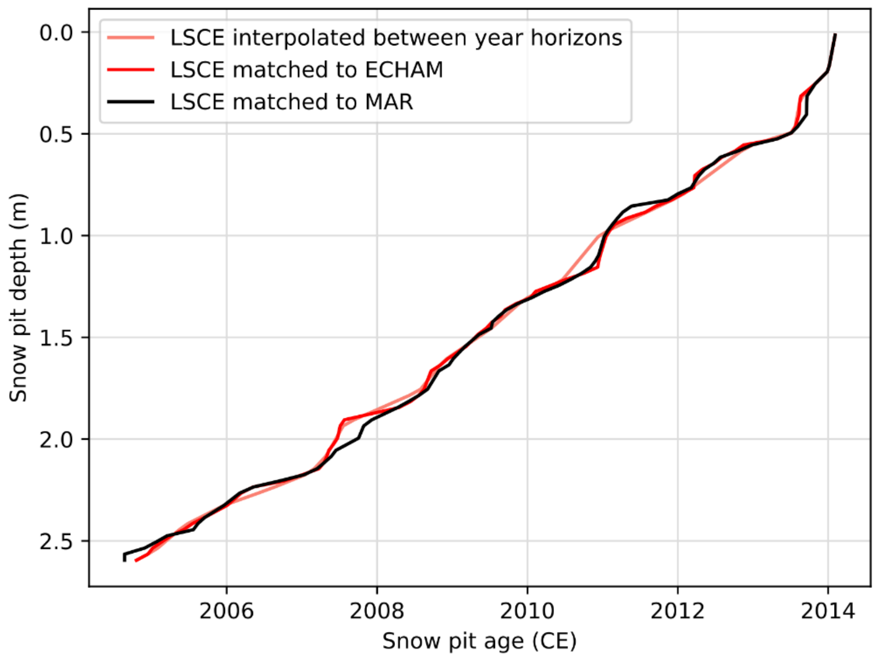

Supplementary Figure 6. Three age models for the LSCE snow pit: interpolated between year horizons (salmon), matched to ECHAM5-wiso (red), and matched to MAR (black).

The differences between the age models are shown in Supplementary Figures 7 and 8.

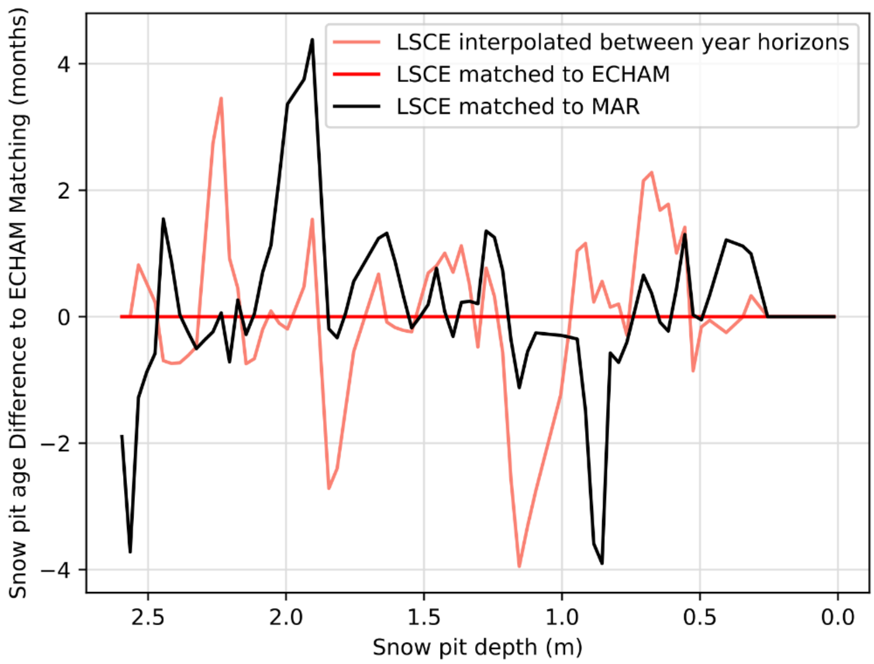

Supplementary Figure 7. Differences between the LSCE age model matched to ECHAM5-wiso and LSCE interpolated between year horizons (salmon), and LSCE matched to MAR (black).

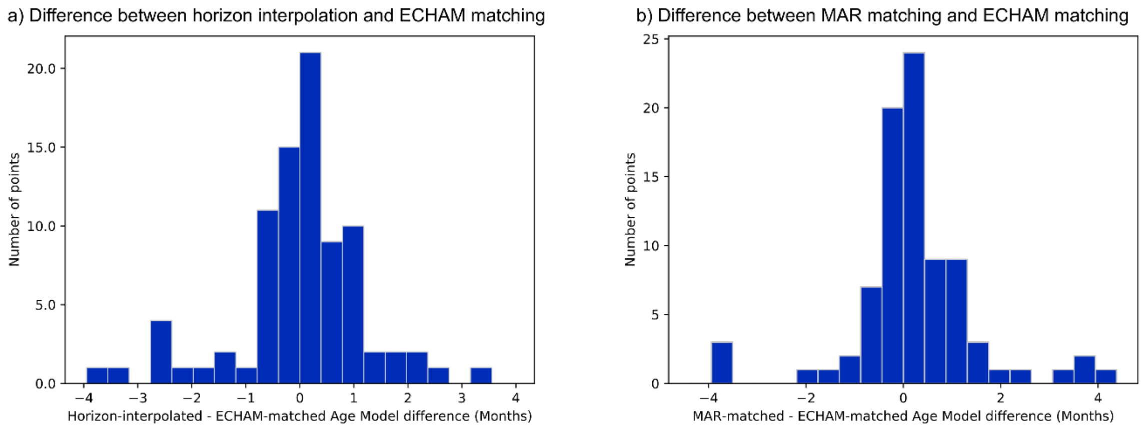

Supplementary Figure 8. Distribution of differences between the LSCE age model matched to ECHAM5-wiso and (a) LSCE interpolated between year horizons, and (b) LSCE matched to MAR.

We chose to retain the ECHAM5-wiso matched age model, as ECHAM specifically models the $\delta^{18}O$. The other dating attempts results in age-differences of up to 4 months, but the difference is mostly lower than 1 month. The uncertainties due to the surface roughness, estimated to 4 months, exceed the difference introduced here with the matching.

Dating of the DRI short core $\delta^{18}O$ was matched to ECHAM5-wiso with the same method, for the 1979-2014 period. Points pre-dating 1979 kept their original dating based on year horizon interpolation, but are not discussed in this article. Because AAD Snow pit $\delta^{18}O$ is very similar to LSCE snow pit $\delta^{18}O$, we tied AAD snow pit to LSCE snow pit using the matching method, rather than tying AAD Snow pit to ECHAM5-wiso outputs. By doing so, we avoid the risk of tying unclear transitions to two different events of ECHAM5-wiso $\delta^{18}O$, and preserve the consistency between the two snow pits.

Globally, the matching process forces measured extrema of $\delta^{18}O$ to be simultaneous to those of the model, in addition to matching the duration of the warm and cold seasons, within the uncertainty of the dating caused by surface roughness. It results in higher correlation with the models, and clarifies the identification of large synoptic events in the snow $\delta^{18}O$.

Supplementary Figures and Tables

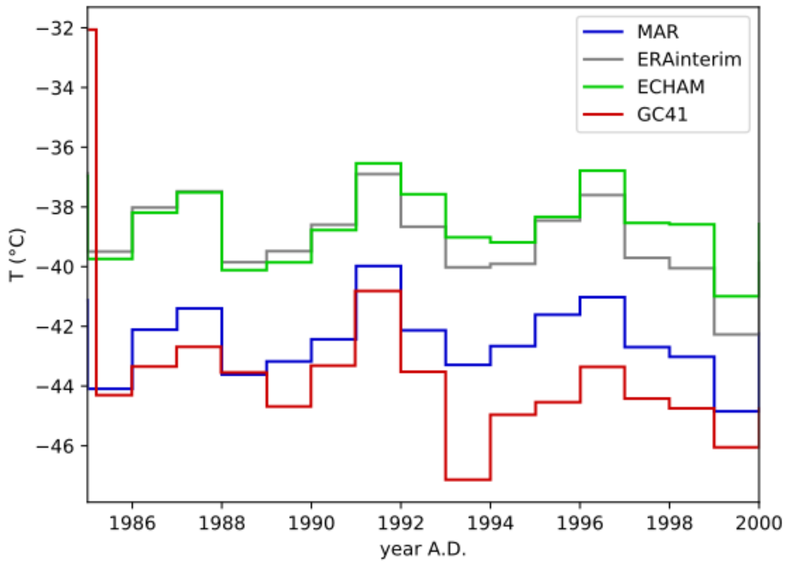

Supplementary Figure 9. Comparison of annual mean temperatures from automatic weather station GC41 (71.60°S, 111.26°E) and 2 m temperature of corresponding grid points in MAR, ERA-interim, ECHAM5-wiso. The automatic weather GC41 station gets buried in snow from 1993.

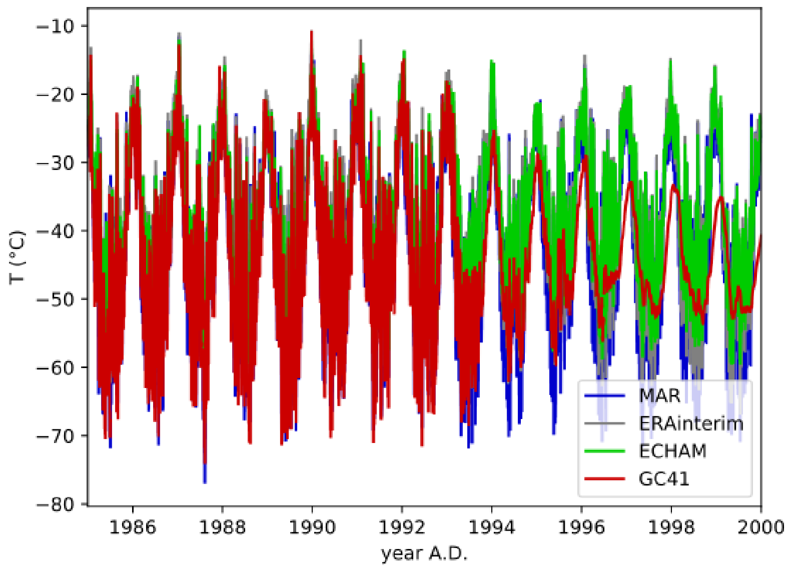

Supplementary Figure 10. Comparison of daily mean temperatures from automatic weather station GC41 (71.60°S, 111.26°E) and 2 m temperature of corresponding grid points in MAR, ERA-interim, ECHAM5-wiso. The automatic weather station gets buried in snow from 1993, causing the smoothing of temperatures on the red curve (GC41).

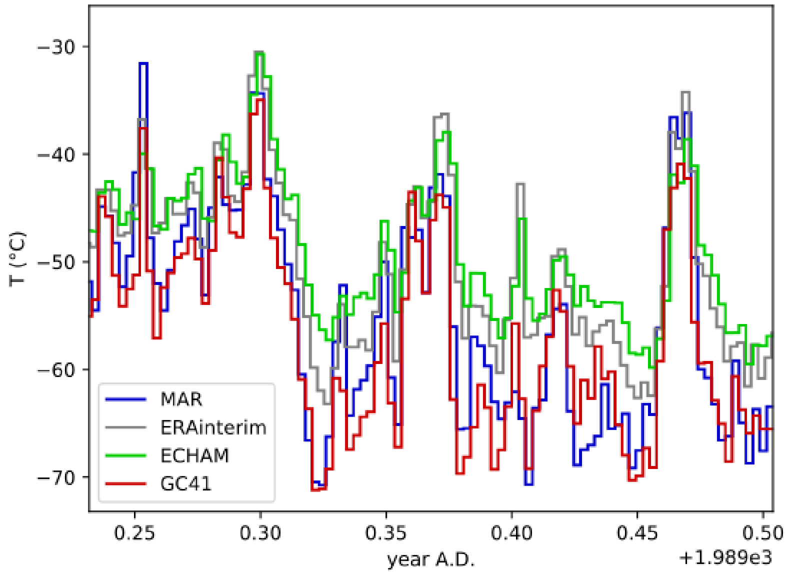

Supplementary Figure 11. Comparison of daily mean temperatures from automatic weather station GC41 (71.60°S, 111.26°E) and 2 m temperature of corresponding grid points in MAR, ERA-interim, ECHAM5-wiso, zoom on a part of the winter of 1989.

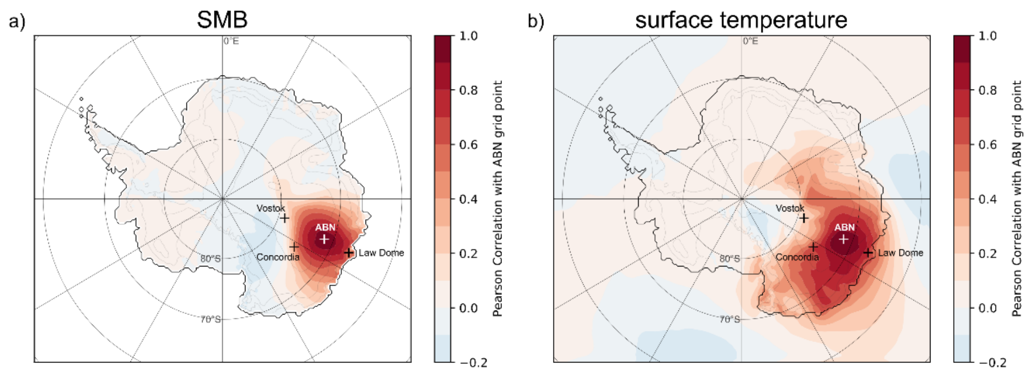

Supplementary Figure 12. (a) Daily Surface Mass Balance (Precipitation – Evaporation) correlation map with Aurora Basin North (white cross). **(b)** Daily surface (2 m) Temperature anomaly correlation map with Aurora Basin North (white cross). Temperature anomalies have been computed as the difference to a 30-day rolling mean of seasonal temperatures. The statistics have been computed from MAR outputs on the 1979-2015 period.

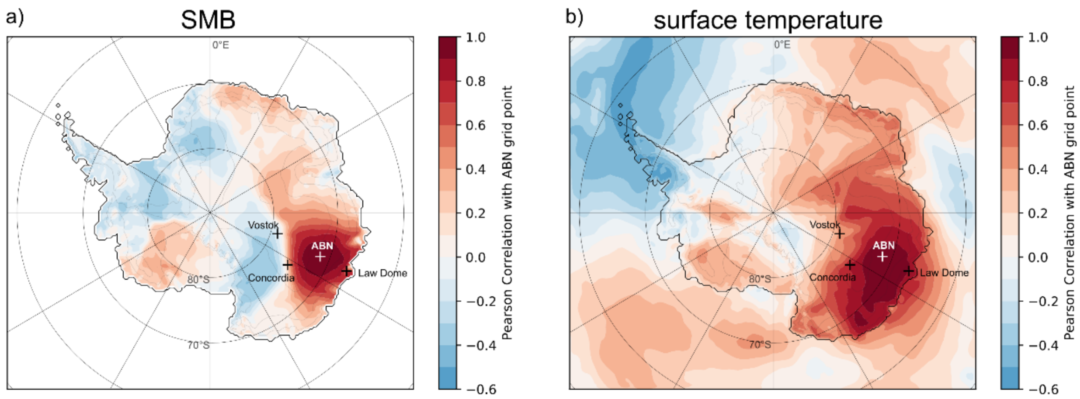

Supplementary Figure 13. (a) Yearly summed Surface Mass Balance (Precipitation – Evaporation) correlation map with Aurora Basin North (white cross). **(b)** Yearly averaged surface (2 m) Temperature correlation map with Aurora Basin North (white cross). The statistics have been computed from MAR outputs on the 1979-2015 period.

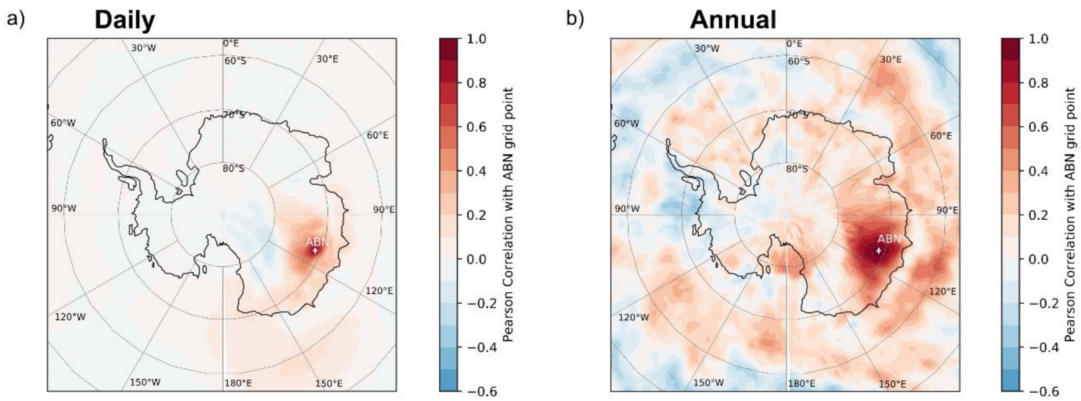

Supplementary Figure 14. (a) Daily precipitation $\delta^{18}O$ correlation map with Aurora Basin North (white cross). **(b)** Yearly snowfall-weighted mean $\delta^{18}O$ correlation map with Aurora Basin North (white cross). The statistics have been computed from ECHAM5-wiso outputs on the 1979-2015 period. $\delta^{18}O$ of the precipitation only takes non-null value when there is precipitation on the site, so the correlation is constrained by the occurrence of precipitations.

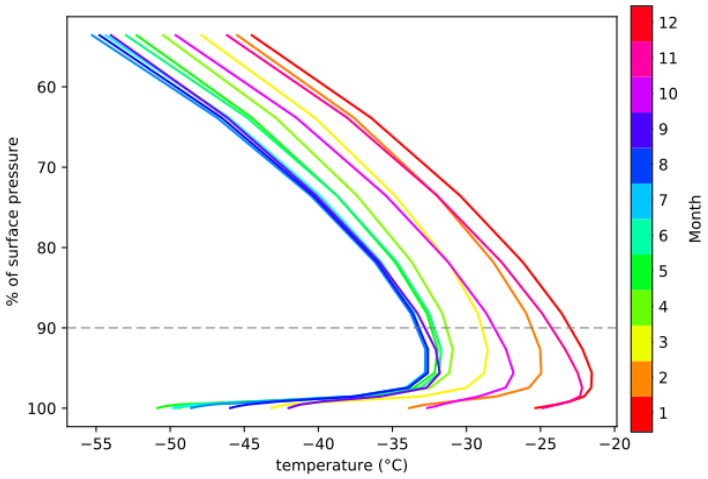

Supplementary Figure 15. Monthly vertical profiles of temperature in MAR. The dashed line at 90% of surface pressure indicates the pressure level used in the main article to compute temperature biases.

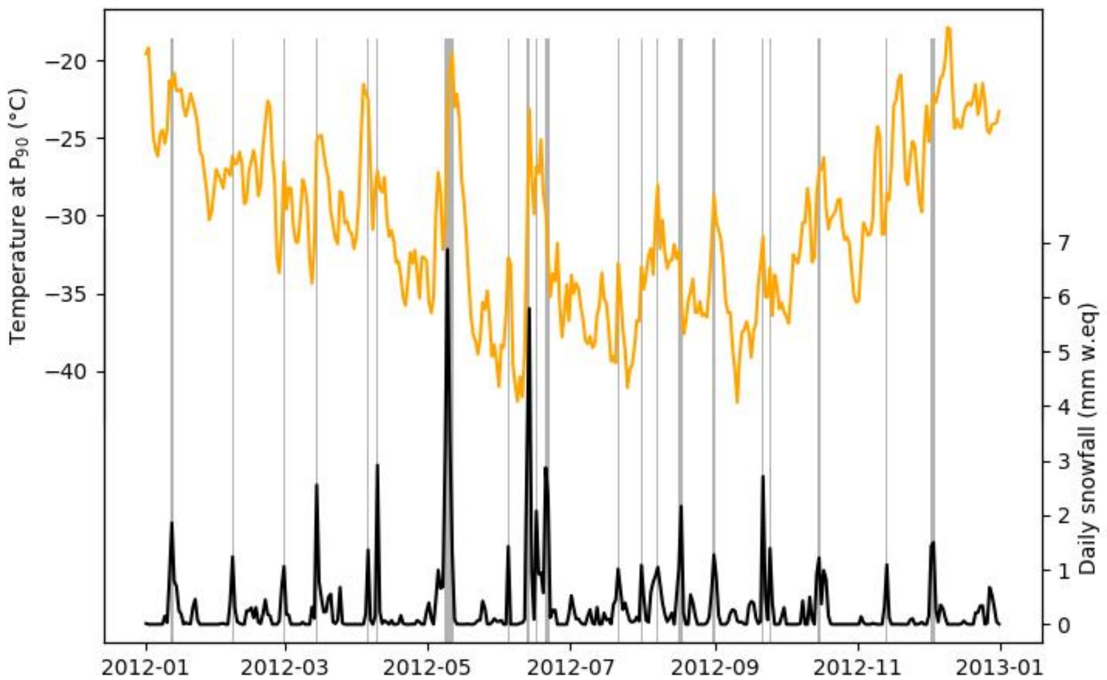

Supplementary Figure 16. MAR temperature (orange), and daily snowfall (black) during the year 2012. Intense snowfall events (larger than 1mm w.eq. day^{-1}) are highlighted with grey shading.

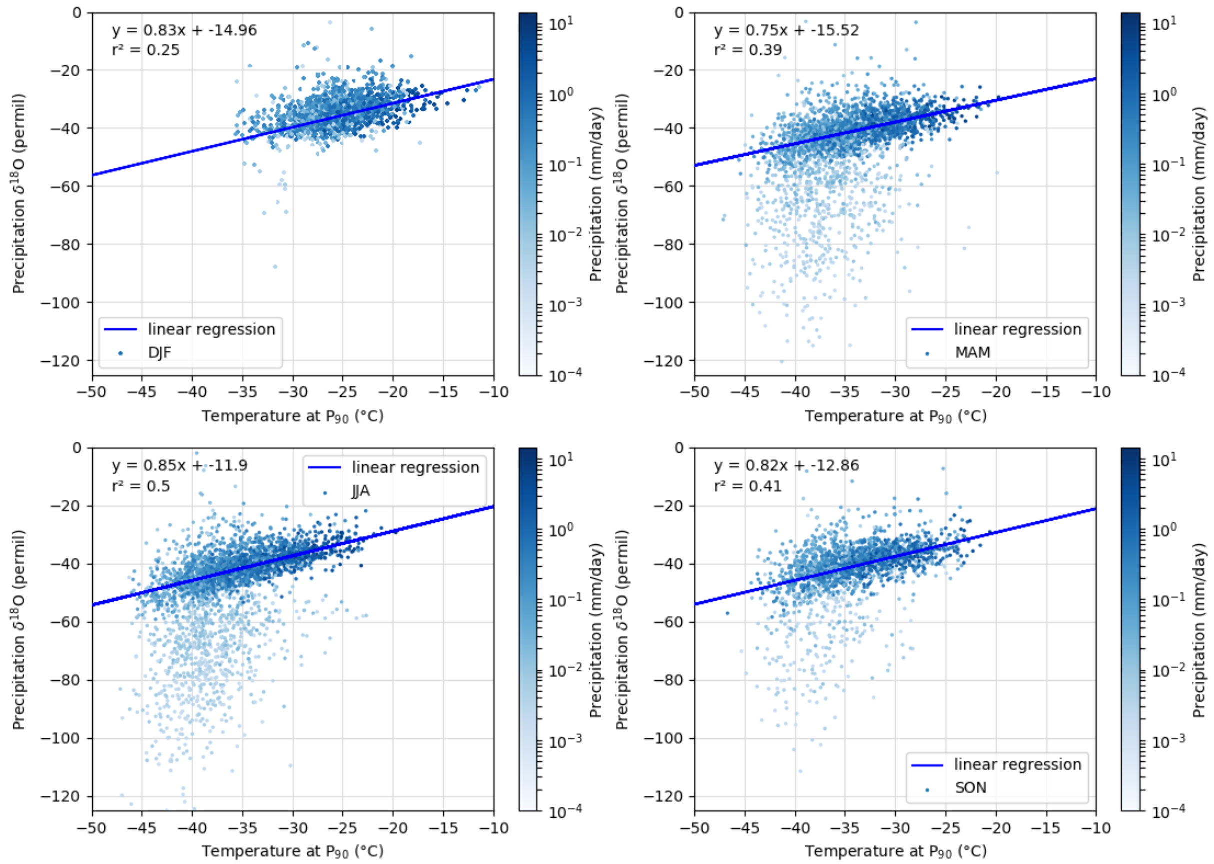

Supplementary Figure 17. Same as Figure 6, but for each of the four seasons.

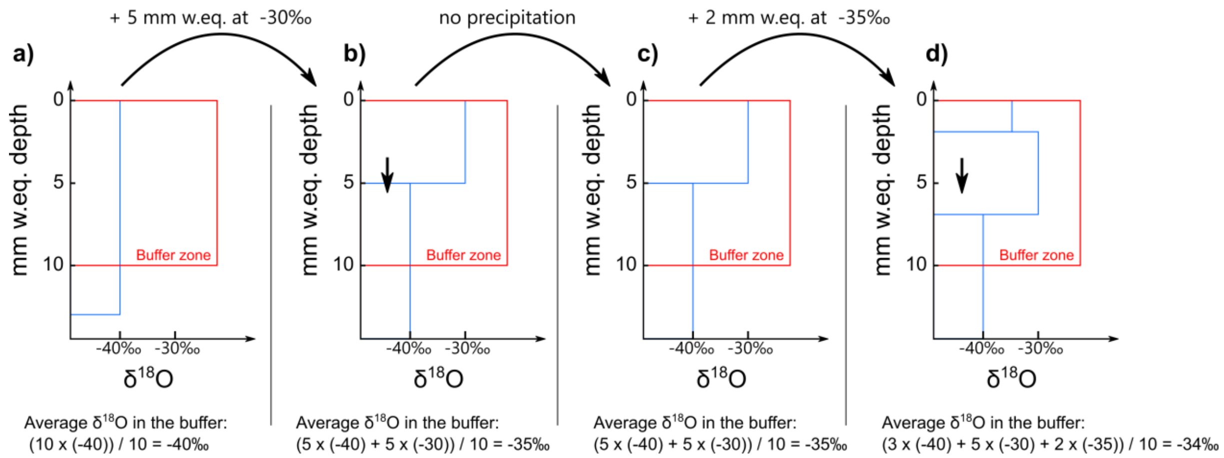

Supplementary Figure 18. Diagram illustrating the average in the surface snow buffer in ECHAM5-wiso. The $\delta^{18}O$ in the buffer zone, which corresponds to the last 10 mm w.eq. of snowfall, is averaged and gives the value of the surface snow $\delta^{18}O$. In case of a snowfall event, e.g. between **(a)** and **(b)**, a layer of thickness equivalent to the snowfall in mm w.eq. is added to the snow surface, with its $\delta^{18}O$

value, and the rest of the snow is pushed downwards. If there is no snowfall, e.g. between **(b)** and **(c)**, the average value remains the same as previously.

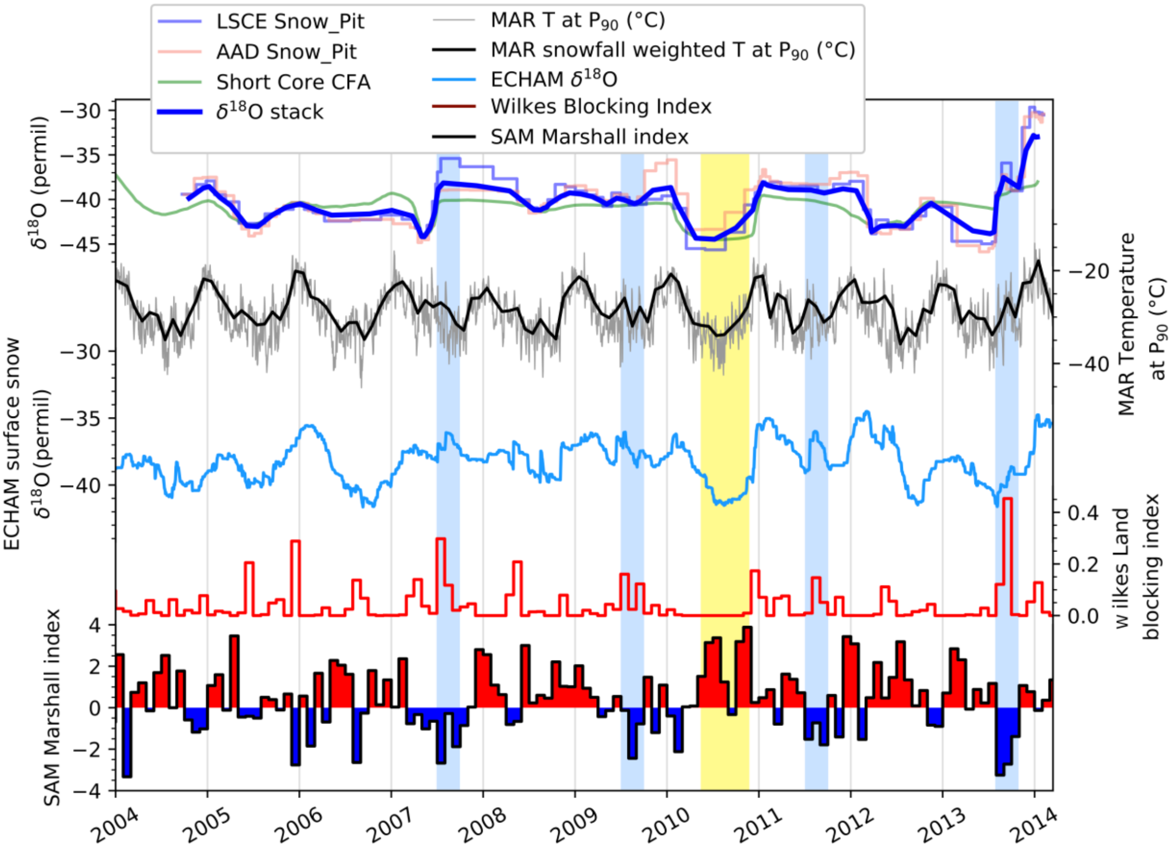

Supplementary Figure 19. Same as Figure 7, with a stack of the three snow δ^{18}O records.

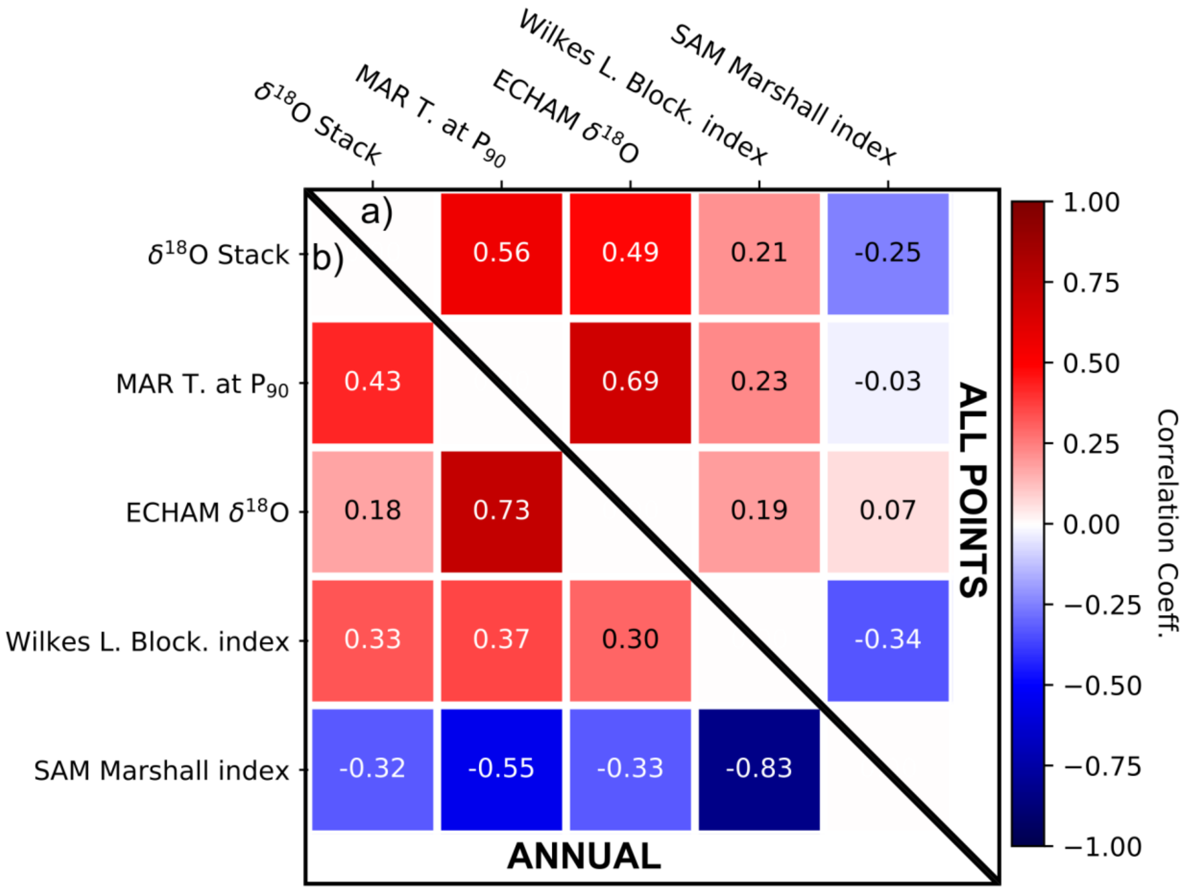

Supplementary Figure 20. Same as Figure 8, with the stack of the three snow $\delta^{18}O$ records.

Supplementary Table 1. Comparison of snow accumulation for the three snow records, and MAR surface mass balance (SMB). All values are given in mm w.eq. year^{-1}. MAR simulates a SMB of 118 mm w.eq. calculated for the period 1979-2013 is in agreement with our accumulation from the short core of 119 mm w.eq. calculated over the same 1979-2013 period. On a multi-year average, the accumulation is very consistent between model SMB and snow accumulation records. However, in a year-to-year comparison, the accumulation can differ largely between our record (DRI short core) and the MAR model, but also between the DRI short core and the snow pit, taken at a ~200 m distance.

	SNOW ACCUMULATION DATA				MAR SMB	MODEL-DATA DIFFERENCE		CROSS-SITE DIFFERENCE	
	DRI	LSCE	AAD	Stack	MAR	(DRI-MAR) /DRI	(Stack-MAR) /Stack	(LSCE-DRI) /LSCE	(LSCE-AAD) /LSCE
2005-2013 mean	102.2	100.4	100.5	101.1	110.0	-7.6%	-8.9%	-1.8%	-0.1%
2005-2013 std	± 34.3	± 19.	± 22.5	± 18.3	± 19.8				

1992-2013 mean	120.9				115.7	4.3%			
1992-2013 std	± 37.4				± 22.7				
1979-2013 mean	118.7				118.1	0.5%			
1979-2013 std	± 33.1				± 21.9				
1969-2013 mean	119.8								
1969-2013 std	± 33.2								
Yearly Accumulation									
2015					107.9				
2014					88.8				
2013	90.5	119.6	136.1	115.4	99.8	-10%	13%	24%	-14%
2012	148.8	110.5	96.1	118.5	111.9	25%	6%	-35%	13%
2011	74.9	95.7	103.5	91.4	89.4	-19%	2%	22%	-8%
2010	113.5	96.2	89.8	99.8	102.1	10%	-2%	-18%	7%
2009	37.3	105.1	86.2	76.2	155.9	-318%	-105%	65%	18%
2008	81.5	103.9	103.7	96.4	104.1	-28%	-8%	22%	0%
2007	153.4	128.5	114.2	132.0	111.1	28%	16%	-19%	11%
2006	107.2	59.6	53.0	73.3	88.0	18%	-20%	-80%	11%
2005	113.1	84.8	122.3	106.7	128.0	-13%	-20%	-33%	-44%
2004	102.3	55.6	55.1	71.0	117.3	-15%			
2003	143.0				105.6	26%			
2002	104.5				117.9	-13%			
2001	107.9				166.5	-54%			
2000	137.4				113.6	17%			
1999	123.4				77.0	38%			
1998	89.9				120.3	-34%			
1997	117.6				86.7	26%			
1996	137.4				147.3	-7%			
1995	154.6				121.3	22%			
1994	118.1				112.8	5%			
1993	189.7				115.6	39%			
1992	212.7				153.1	28%			
1991	111.9				126.0	-13%			
1990	147.2				98.7	33%			
1989	119.4				109.0	9%			
1988	101.3				111.0	-10%			
1987	77.6				117.2	-51%			
1986	88.9				114.6	-29%			
1985	141.7				106.9	25%			
1984	127.4				131.8	-3%			
1983	97.5				112.1	-15%			
1982	153.4				143.0	7%			
1981	93.5				170.8	-83%			
1980	138.6				144.2	-4%			

1979	97.0	102.5	-6%
1978	119.6		
1977	118.4		
1976	121.7		
1975	179.9		
1974	74.8		
1973	96.4		
1972	96.6		
1971	115.9		
1970	184.3		
1969	130.3		

References

Boggs, P. T., Byrd, R. H., Rogers, J. E., & Schnabel, R. B. (1992). *User's reference guide for odrpack version 2.01: Software for weighted orthogonal distance regression*. https://doi.org/10.6028/NIST.IR.4834

Cole-Dai, J., & Mosley-Thompson, E. (1999). The Pinatubo eruption in South Pole snow and its potential value to ice-core paleovolcanic records. *Annals of Glaciology*, *29*, 99-105. https://doi.org/10.3189/172756499781821319

Ginot, P., Dumont, M., Lim, S., Patris, N., Taupin, J.-D., Wagnon, P., Gilbert, A., Arnaud, Y., Marinoni, A., Bonasoni, P., & Laj, P. (2014). A 10 year record of black carbon and dust from a Mera Peak ice core (Nepal): variability and potential impact on melting of Himalayan glaciers. *The Cryosphere*, *8*(4), 1479-1496. https://doi.org/10.5194/tc-8-1479-2014

Johnsen, S. J., Clausen, H. B., Cuffey, K. M., Hoffmann, G., Schwander, J., Creyts, T., & Hondoh, T. (2000). Diffusion of stable isotopes in polar firn and ice : the isotope effect in firn diffusion. *Physics of Ice Core Records*, 121-140.

McConnell, J. R., Lamorey, G. W., Lambert, S. W., & Taylor, K. C. (2002). Continuous Ice-Core Chemical Analyses Using Inductively Coupled Plasma Mass Spectrometry. *Environmental Science & Technology*, *36*(1), 7-11. https://doi.org/10.1021/es011088z

Sigl, M., Fudge, T., Winstrup, M., Cole-Dai, J., Ferris, D., Mcconnell, J., Taylor, K., Welten, K., Woodruff, T., Adolphi, F., Bisiaux, M., Brook, E., Buizert, C., Caffee, M., Dunbar, N., Edwards, R., Geng, L., Iverson, N., Koffman, B., … Sowers, T. (2016). The WAIS Divide deep ice core WD2014 chronology - Part 2: Annual-layer counting (0-31 ka BP). *Clim. Past*, 19. https://doi.org/10.5194/cp-12-769-2016